IL NUOVO CIMENTO Vol. 35 C, N. 5 Settembre-Ottobre 2012
DOI 10.1393/ncc/i2012-11317-3

Communications: SIF Congress 2011

Magnetic Tunneling Junctions for biosensors: From the growth to the detection

D. Petti(*)

LNESS, Dipartimento di Fisica, Politecnico di Milano and CNISM via Anzani 42, 22100 Como, Italy

ricevuto il 16 Gennaio 2012; revisionato l' 11 Aprile 2012; approvato il 18 Aprile 2012

Summary. — In the last ten years, magnetoelectronics has emerged as a promising new platform technology for biosensor and biochip development. In particular, magnetoresistive-based sensors, conventionally used as read heads in hard disk drives, have been used in combination with biologically functionalized magnetic labels to demonstrate the detection of molecular recognition. In this paper, the growth and fabrication of spintronic transducers based on the magnetoresistance of tunneling magnetic junctions are described. Moreover the detection of 250 nm streptavidin magnetic beads is presented.

PACS 87.85.fk – Biosensors.
PACS 87.85.Rs – Nanotechnologies-applications.
PACS 85.75.Ss – Magnetic field sensors using spin polarized transport.

1. – Introduction

A common approach to detect biological molecules is to attach to the target molecule a label that produces an externally observable signal. Recently, a detection method for biorecognition based on magnetic markers and magnetoresistive sensors has been developed [1]. The markers are specifically attached to the target molecules, and their magnetic stray field is picked up by embedded magnetoresistive sensors as a change of electrical resistance. Magnetic biosensors were made possible by the fast development of devices based on physical effects that relate an electrical resistance to external magnetic fields, namely the giant magnetoresistance (GMR) [2, 3] and the tunnelling magnetoresistance (TMR) [4,5]. TMR is a magnetoresistive effect which occurs in magnetic tunnel junctions and it is defined as $(R_\perp - R_\parallel)/R_\parallel$, where $R_\parallel$ and $R_\perp$ are the tunnel resistance of the junction when the magnetizations of the two electrodes are aligned parallel and antiparallel, respectively. In particular in 2004, TMR over 200% was reported for coherent

(*) E-mail: daniela.petti@mail.polimi.it

tunnelling in crystalline fcc (100) MgO barriers [6,7]. In most of these studies, transition metal ferromagnetic electrodes are used (CoFe, CoFeB, Fe). These high TMR values together with the direct electronic translation of the change of magnetic configuration, compatibility with standard CMOS (Complementary Metal-Oxide Semiconductor) processing and scalability opened a realm of practical applications, among which, the most important are non-volatile magnetic tunnel junction random access memories (MRAM), spin tunnel read heads [8] and now magnetoresistive biosensors.

Compared to the established fluorescent detection method, magnetic biosensors have a great number of advantages [9]. First of all, the magnetic properties of the beads are stable over time, because the magnetism is not affected by reagent chemistry or subject to photo-bleaching (a problem with fluorescent labelling); in addition, magnetic particles give the possibility of manipulation and sorting biological entities [10]. Secondly, current portable biosensors, essentially based on fluorescence, do not permit to reach very high biological sensitivity without the use of amplification processes like PCR (Polymerase Chain Reaction), which can introduce biases and spurious effects in the assay. In contrast, magnetic labels in combination with highly sensitive spintronic biosensors offer the opportunity to reach sensitivities in the sub aM range, as has been already reported by a group [11]. Fast performance, integrability in conventional electronic platforms, miniaturization, scalability and portability makes this magnetic detection system a promising choice for the detection units of future widespread and easy to use lab-on-a-chip systems or biochips [12, 13]. In particular, compared to GMR sensors, which have extensively studied as biosensors, MgO-based magnetic tunnel junctions offer higher magnetoresistance (MR) ratios and therefore higher magnetic field sensitivity, but slightly higher noise levels [14]. As a result, MTJs are better suited for the accurate detection of the small magnetic fields (in the range of pT [15]) which are typically encountered in most biomagnetic applications. In the following, I will present the optimization of the MTJ growth, the device fabrication and a new experimental scheme which exploits the focussing action of the self-field generated by the current flowing in the sensor and the stray field coming from the free magnetic layer to detect superparamagnetic nanoparticles.

2. – Experimental

Magnetic tunneling junction (MTJ) sensors have been deposited in a high vacuum ($1 \cdot 10^{-9}$ Torr) magnetron sputtering system (AJA ATC orion 8 system) under a magnetic field of 30 mT in order to induce parallel easy axis in both pinned and free layers. The stack structure is (thickness in Ångstrom): Si/ SiO_2(1000)/ Ta(50) / Ru(180)/ Ta(30) / $Ir_{22}Mn_{78}$(200) / $Co_{40}Fe_{40}$(20) / Ru(9) / $Co_{40}Fe_{40}B_{20}$(30) / MgO(20) / $Co_{40}Fe_{40}B_{20}$(30) / Ru(50) / Ta(50). Co-Fe and MgO layers have been deposited in r.f. mode and the other layers have been deposited in d.c. mode. Devices with rectangular shape and dimension of $2.5 \times 120\,\mu m^2$ have been fabricated by optolithography, with the shorter side parallel to the easy axis of the pinned layer. After e-beam evaporation of Cr(80 Å)/Au(3000 Å) contacts, the samples have been annealed at 250 °C at a pressure of 10^{-6} Torr for 1 h in a magnetic field of 400 mT applied along the short side (easy axis of the pinned layer). Then, a 2000 Å thick layer of SiO_2 has been deposited in r.f. mode from a SiO_2 target as protective coating. On top of the chip is mounted a click-on microfluidic system [16,17]. In the experimental set-up the sensor chip with 8 tunnel junctions is centered between two coils and one electromagnet, which are placed orthogonally in such a way that the longitudinal direction of the sensor strip is aligned with a d.c. field Hl and the transverse direction parallel to an a.c. or d.c. bias field Hb. In this configuration, the sensor is

TABLE I. – *Power, Ar pressure, deposition rate and surface roughness of the stack layers for optimized magnetron sputtering deposition.*

Layer (Å)	Power (W)	Ar pressure (mTorr)	Dep. rate (Å/min)	Rough. RMS (Å)
Ta (50)	100 DC	3	43	below 1
Ru (50)	50 DC	3	24	below 1
Ta (30)/Ru (180)/Ta (50)	opt. cond.	opt. cond.		2.5
IrMn (10)	50 DC	3	28	1.1
FeCo (5)	200 RF	12		1
FeCoB (5)	58 DC	3	13	1
MgO (2)	220 RF	2	4.5	below 1
CoFeB (30)/MgO (20)	opt. cond.	opt. cond.		below 1

linearized by the d.c. field Hl and biased to the most sensitive point of its characteristic by Hb. This field, in combination with the self-field generated by the current flowing through the junction, magnetize also the superparamagnetic nanoparticles. A multiplexing system (MUX) is used to address the eight different junctions in such a way that the current is permanently flowing throughout all the junctions (for stability purpose) and the readout occurres sequentially. An AC current generated by a Keithley 6221 is injected into the sensors and the voltage signal is collected through a lock-in amplifier (HF2LI, ZI).

3. – Results and discussion

3˙1. *Growth and device fabrication.* – The roughness of the layer interfaces in magnetic tunnel junctions is an important factor that greatly influences the performance of the junctions [5]. Improvement of the roughness at the interface with the barrier could enhance the local spin-dependent transport of the conduction electrons through tunneling and the MR would be increased consequently. Therefore the layers roughness has been carefully optimized by checking the surface topology by Atomic Force Microscopy (AFM) measurements (Veeco Innova). RRMS (Root Mean Square Roughness) values were obtained from $1 \times 1\,\mu m^2$ surface topology image, acquired in tapping mode. Single layers of thickness comparable to those of the final stack have been grown on a Si substrate in different conditions. Three parameters has been taken into account: Ar pressure deposition, power applied to the targets, substrate-sample distance. In table I a summary of the optimized parameter and their corresponding roughness for each film are listed. Importantly, the surface of the whole buffer layer (Ta/Ru/Ta) results smooth with a roughness RRMS = 2.5 Å; note that a correct design of the buffer layer favors the crystallization of the bottom CoFeB layer, which is also influenced, other than by the texturation of the MgO barrier, by the crystalline structure of other underlying layers such as the pinning antiferromagnet [18]. Indeed, such a structure gives rise to a strong [111] texture of IrMn, as confirmed by X-Ray Diffraction (XRD) measurements (data not shown [20]), which also induces an improvement of the exchange bias of CoFe [19] (in this case of about 1000 Oe). In the inset of fig. 1 the AFM image of 2 nm MgO surface is presented. The roughness RMS reported in table I is below 1 nm, that is also the value presented by the entire CofeB/MgO bilayer. Also in this case XRD shows that the MgO texturation is [001] as those of FeCoB, which leads to coherent electron tunneling

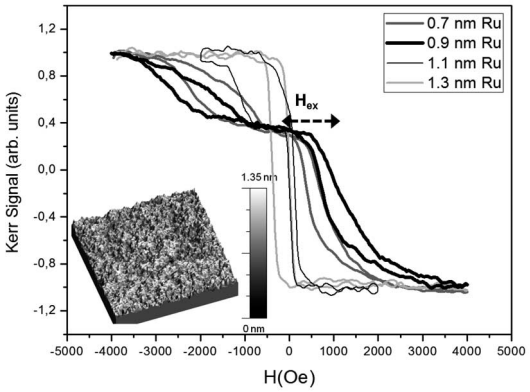

Fig. 1. – Hysteresis loops along the easy axis direction for SAF structures with different Ru thicknesses; the loop separation ($H_{\rm ex}$), proportional to the bilinear exchange coupling, is observed to be 1000 Oe in the structure with 0.9 nm Ru. In the inset of the figure: AFM image of the MgO layer ($1 \times 1\,\mu{\rm m}^2$) grown in the optimized conditions of table I.

through the barrier and hence devices with tunnelling magnetoresistance (TMR) values as high as 100% [5, 7, 6].

In order to achieve a linearized, hysteresis-free sensor response, different parameters of the free FeCoB layer must be considered [21]: layer thickness, shape anisotropy and thermal annealing. In this case the linearity is achieved using the shape anisotropy given by the devices size [17] and the effect of an external linearizing magnetic field. The pinning of the botton layer is achieved instead through synthetic antiferromagnet (SAF); indeed CoFeB bottom layer is pinned antiferromagnetically to CoFe through a Ru spacer by bilinear exchange coupling, while CoFe is in turn directly pinned by exchange bias with an antiferromagnet. The antiferromagnet used is IrMn because it provides both high exchange bias magnitudes and good thermal stability [22]. There are three major advantages for using a SAF pinned layer; first of all, it significantly reduces the stray fields from the pinned layer, which sometimes acts as an undesirable extra external field on the free layer altering the response of the sensor; secondly, it enhances the pinning of the bottom layer and finally it improves the sensor thermal stability because the Ru layer acts as a barrier against Mn interdiffusion [23] in MgO. To achieve a stable bilinear coupling between FeCoB and FeCo, the Ru thickness must be carefully optimized: in fig. 1 the hysteresis loops for the annealed heterostructure Ta(50) / Ru(180)/ Ta(30) / $Ir_{22}Mn_{78}$(200) / $Co_{40}Fe_{40}$(20) / Ru(x) / $Co_{40}Fe_{40}B_{20}$(30)/MgO(20) are shown. x corresponds to 7, 9, 11, 13 Å (respectively, dark grey, black, thin black and light grey lines). The hysteresis loops have been recorded by employing the Magneto Optical Kerr Effect (MOKE) in the longitudinal configuration; the light is modulated by a PhotoElastic Modulator (PEM) at 50 kHz and the signal from the photodiode demodulated by a lock-in amplifier [24]. The important parameter to observe is the loop separation ($H_{\rm ex}$) that is proportional to the bilinear coupling [25]: with 9 Å of spacer it is 1000 Oe, with 7 Å and 11 Å it decreases to 600 and 50 Oe, respectively. With 13 Å of Ru the coupling becomes ferromagnetic, as expected by the oscillatory behavior of the bilinear coupling [26].

In the bottom panel of fig. 2, a schematic of the chip is presented: each of the eight MTJ sensor is provided with two independent contacts for the bottom and top electrodes,

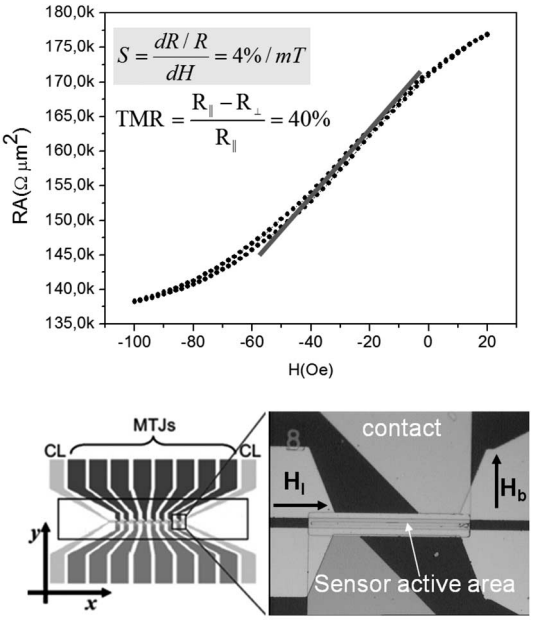

Fig. 2. – Top panel: sensor transfer curve measured with $I_s = 100\,\mu$A. Bottom panel: on the left, schematic of the chip with eight MTJ sensors and two current lines for beads excitation; the rectangle indicates the outline of the microfluidic channel. The optical image of a single MTJ sensor is shown on the right, with the direction of the two applied magnetic fields (Hl and Hb).

while there are two independent current lines (CL). On the right, on the optical image of the sensor the linearizing (Hl) and the biasing (Hb) magnetic fields are indicated. The sensor response (top panel of fig. 2) is linear due to the combined effect of the shape anisotropy and the bias field. By applying 0.2 mT of Hl the hysteresis of the transfer curve disappears, while magnetoresistance decreases from roughly 100% to 40%, resulting in a low-field sensitivity $S_0 = (R\mu_0)^{-1}(\mathrm{d}R/\mathrm{d}H_y)$ of 4.4%/mT with $I_s = 100\,\mu$A and RA product of about 140 kΩ.

3˙2. *Beads detection.* – The experiment has been performed with Nanomag-D beads (Micromod, Rostock, Germany) with a nominal diameter of 250 nm, diluted with deionized water until reaching the concentration of 0.3 mg/ml, in order to study the sedimentation time of the beads under the focusing action of the sensor self-field and stray field. The beads are injected by means of a syringe pump with a rate of 50 μl/min and magnetized using an in-plane, transverse, continuous field of 1.4 mT. During the beads sedimentation the combined action of the AC current flowing through the sensor ($I_s = 100\,\mu$A, $f = 39$ kHz) and the stray field coming from the free magnetic layer of the sensor focuses the beads on the top and on the sides of the junction, as can be seen in fig. 3, which is the optical microscope image of the beads distribution taken after beads sedimentation and hybridization to the biotynilated sensor surface. After sedimentation deionized water is injected in the microfluidic channel at a rate of 150 μl/min for washing.

In this configuration the beads sedimentation is completely concluded in about 20 minutes, as the data presented in fig. 4 panel a) confirm. The first harmonic in phase signal [17] presents a very high signal/noise ratio due to the modulation of the current

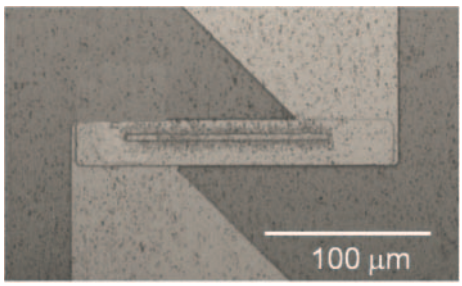

Fig. 3. – Optical image of the beads distribution after sedimentation and hybridization biotyn-streptavidin.

which contributes to the suppression of the $1/f$ noise component [27]. The bead injection produces a decreasing of the voltage signal, which can be explained if one calculates the average magnetic field sensed by the junctions. Three contributions must be taken into account: the biasing external field Hb, the field from the magnetic nanoparticles and the demagnetizing field coming from the free magnetic layer of the sensor itself. In particular the first two components can be easily simulated [28] as depicted in fig. 4 panel b), in which the average field sensed by the junctions for a monolayer of beads located at $0.5\,\mu$m

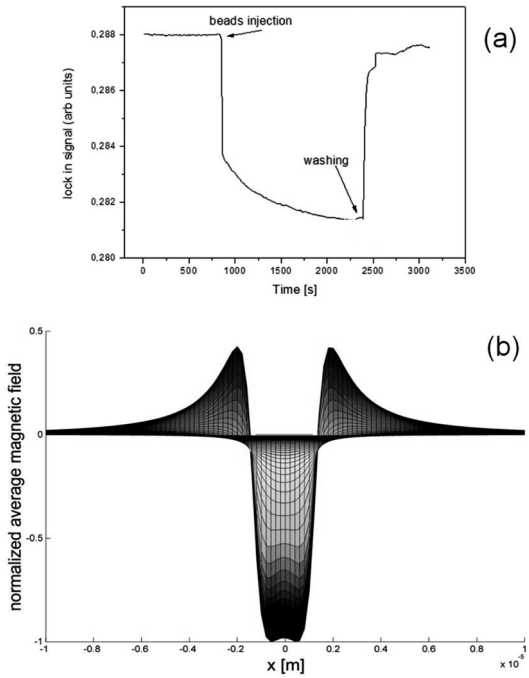

Fig. 4. – Panel a: first harmonic in phase signal coming from the beads sedimentation and washing; the current injected in the sensor is $100\,\mu$A with $f = 39\,$kHz; a DC field of 14 Oe is applied transverse to the sensor. Panel b: average magnetic field calculated from a continuous distribution of beads covering an area larger than the sensor (this last being centered in 0 and $2\,\mu$m wide).

of height and magnetized by a transverse-in plane field of 14 Oe is shown as a function of the beads position. Note that beads outside the sensor contribute with a positive sign, while beads inside the sensor with a negative one. If the distribution is homogenous and infinitively extended, the average field should be positive and very low. In this case the optical image of fig. 3 shows that the beads are mostly attracted on the top and on the side of the sensor by the self and stray field, giving rise to a negative contribution; in this configuration the positive sensitivity of the sensor gives rise to a decrease of the signal. After the washing, the signal in fig. 4 recovers the initial baseline: indeed, in this experiment, the surface of the sensor is plain, no immobilization of the beads takes place and water pushes away the nanoparticles in the microfluidic channel. The recovery of the initial baseline confirms that in this configuration any sensor drift happens.

4. – Conclusion

In this paper the most critical issues of magnetoresistive transducer fabrication are presented. In the bead detection experiment, the modulation of the current flowing through the sensor has been performed in order to bring a good suppression of $1/f$ noise. In this configuration, the combination of the self-field generated by the current and the demagnetizing field favors the beads sedimentation which takes only 20 minutes. Moreover the beads distribution resulting from the focusing action of the self and stray field gives rise to average field contributions of the same sign, so finally to an enhancement of the beads signal. These results pave the way towards a new simplified detection scheme, in which the self-field of the sensor can be exploited.

* * *

This work was supported by Fondazione Cariplo via the project SpinBioMed (Project No. 2008.2330). The author thanks R. Bertacco, E. Albisetti, M. Leone of LNESS center, Dipartimento di Fisica of Politecnico di Milano for working in this project. D. Chrastina of LNESS center, Dipartimento di Fisica of Politecnico di Milano for XRD measurements. M. Donolato form CIC nanoGune Consolider, P. Freitas, S. Freitas, R. Chaves and F. Cardoso form INESC-MN (Lisbon) for fruitful discussion and help in the improvement of the lithographic process.

REFERENCES

[1] Megens M. and Prins M., *J. Magn. Magn. Mater*, **293** (2005) 702.
[2] Baibich N. M., Broto J. M., Fert A., Nguyen Van Dau F., Petroff F., Etienne P., Creuzet G., Friedrich A. and Chazelas J., *Phys. Rev. Lett.*, **61** (1988) 2472.
[3] Baibich N. M., Broto J. M., Fert A. and Nguyen F., *Phys. Rev. B*, **39** (1989) 4828.
[4] Jullière M., *Phys. Lett.*, **54 A** (1975) 225.
[5] Butler W. H., Zhang X.-G., Schulthess T. C. and MacLaren J. M., *Phys. Rev. B*, **63** (2001) 054416.
[6] Parkin S. S. P., Kaiser C., Panchula A., Rice P. M., Hughes B., Samant M. and Yang S.-H., *Nat. Mater*, **3** (2004) 862.
[7] Yuasa S., Nagahama T., Fukushima A., Suzuki Y. and Ando K., *Nat. Mater*, **3** (2004) 868.
[8] Tehrani S., Slaughter J. M., Deherrera M., Engel B. N., Rizzo N. D., Salter J., Durlam M., Dave R. W., Janeskly J., Butcher B., Smith K. and Grynkewich G., *Proc. IEEE*, **91** (2003) 703.
[9] Sandhu A., *Nat. Nanotechnol.*, **2** (2007) 746.

[10] Donolato M., Vavassori M., Gobbi M., Deryabina M., Hansen M. F., Metlushko V., Ilic B., Cantoni M., Petti D., Brivio S. and Bertacco R., *Adv. Mater*, **22** (2010) 2706.
[11] Gaster R. S., Xu L., H S.-J., Wilson R. J., Hall D. A., Osterfeld S. J., Yu H. and Wang S. X., *Nat. Nanotechnol.*, **6** (2011) 314.
[12] Graham D. L., Ferreira H. A. and Freitas P. P., *Trends Biotech.*, **22** (2004) 455.
[13] Wang S. X., Bae S.-Y., Li G., Sun S., White R. L., Jennifer T. Kemp and Chris D. Webb, *J. Magn. Magn. Mater*, **293** (2005) 731.
[14] Freitas P. P., Ferreira R., Cardoso S. and Cardoso F., *J. Phys.: Condens. Matter*, **19** (2007) 165221.
[15] Chaves R. C., Freitas P. P., Ocker B. and Maass W., *J. Appl. Phys.*, **103** (2008) 07E931.
[16] Dalslet B. T., Damsgaard C. D., Donolato M., Strømme M., Strömberg M., Svedlindh P. and Hansen M. F., *Lab. Chip.*, **11** (2010) 296.
[17] Donolato M., Sogne E., Dalslet B. T., Cantoni M., Petti D., Cao J., Cardoso F., Cardoso S., Freitas P. P., Hansen M. F. and Bertacco R., *Appl. Phys. Lett.*, **98** (2011) 073702.
[18] Cao J., Kanak J., Stobiecki T., Wisniowski P. and Freitas P. P., *IEEE Trans. Magn.*, **45** (2009) 3464.
[19] Liu H., *Thin Solid Films*, **441** (2003) 111.
[20] Albisetti E., Petti D., Reichlov H., Marti X. and Bertacco R., to be submitted.
[21] Winśiowski P., Almeida J. M., Cardoso S., Barradas N. P. and Freitas P. P., *J. Appl. Phys.*, **103** (2008) 07A910.
[22] Anderson G. W., Pakala M. and Huai Y., *IEEE Trans. Magn.*, **36** (2000) 2605.
[23] Lee Y. M., Hayakawa J., Ikeda S., Matsukura F. and Ohno H., *Appl. Phys. Lett.*, **89** (2006) 042506.
[24] Brivio S., Cantoni M., Petti D. and Bertacco R., *J. Appl. Phys.*, **108** (2010) 113906.
[25] Desai M., Misra A. and Doyle D., *IEEE Trans. Magn.*, **41** (2005) 3151.
[26] Parkin S. S. P., More N. and Roche K. P., *Phys. Rev. Lett.*, **64** (1990) 2304.
[27] Almeida J. M., Ferreira R., Freitas P. P., Langer J., Ocker B. and Maass W., *Appl. Phys. Lett.*, **99** (2006) 08B314.
[28] Hansen T. B. G., Damsgaard C. D., Dalslet B. T. and Hansen M. F., *J. Appl. Phys.*, **107** (2010) 124511.